The Journal of Neuroscience, October 1993, 13(10): 4339–4353

The Contributions of NMDA, Non-NMDA, and GABA Receptors to Postsynaptic Responses in Neurons of the Optic Tectum

Peter W. Hickmott and Martha Constantine-Paton

Department of Biology, Yale University, New Haven, Connecticut 06511

Activation of the NMDA subtype of glutamate receptor has been implicated in activity-dependent development and plasticity in several systems, including the retinotectal system of amphibians. To gain a better understanding of the response properties of tectal neurons, with particular emphasis on the role of both non-NMDA and NMDA glutamate receptors, we have developed an *in vitro* slice preparation of the diencephalon and midbrain of frog (*Rana pipiens*) tadpoles. In these slices, we electrically stimulated the optic tract and recorded both mono- and polysynaptic responses in single tectal neurons using whole-cell voltage clamp or current clamp. By including biocytin in the recording electrode, we were also able to determine the location and morphology of many of these neurons.

Using these techniques, we found that the current–voltage (*I–V*) relations for both mono- and polysynaptic responses of tectal neurons showed voltage dependence only in the presence of extracellular Mg^{2+}. This dependence reflects the hyperpolarization-dependent block of the NMDA channel by Mg^{2+}. Bath application of 6-cyano-7-nitroquinoxaline-2,3-dione, a non-NMDA glutamate receptor antagonist, reduced both mono- and polysynaptic responses of tectal neurons. Bath application of the NMDA receptor antagonist DL-2-amino-5-phosphonovaleric acid (DL-APV) strongly reduced polysynaptic responses. When neurons were depolarized by the voltage clamp, relieving the Mg^{2+}-dependent block of the NMDA channel, DL-APV application also reduced monosynaptic responses. Application of the $GABA_A$ receptor antagonist (−)bicuculline methiodide significantly increased the polysynaptic responses of tectal neurons, reflecting block of inhibition. We further confirmed the presence of these three types of receptors by examining postsynaptic currents evoked by iontophoretic application of the three agonists, NMDA, (*R,S*)-α-amino-3-hydroxy-5-methylisoxazole-4-propionic acid (AMPA), and GABA.

These results confirm that the dominant excitatory transmitter in the tectum appears to be glutamate. Furthermore, the retinotectal synapses (i.e., monosynaptic currents) express functional NMDA receptors that are voltage dependent and are not responsible for the bulk of normal excitatory transmission. Polysynaptic responses, however, are mediated by both non-NMDA and NMDA receptors, and inhibition plays a significant role in sculpting these polysynaptic responses.

[Key words: AMPA receptor, NMDA receptor, GABA receptor, activity-dependent development, map refinement, optic tectum,* Rana pipiens*]

The projections from the retina to the midbrain tectal lobes of nonmammalian vertebrates have been favored systems for studies of development and plasticity in the CNS because of their accessibility throughout development and their regenerative capacity (for reviews, see Udin and Fawcett, 1988; Constantine-Paton, 1990). The development of the retinotectal projection of lower vertebrates has been shown to involve both chemospecific (Bonhoeffer and Huf, 1982; Stahl et al., 1990; for review, see Fraser, 1985) and activity-dependent mechanisms (Meyer, 1982; Reh and Constantine-Paton, 1985; for review, see Udin and Fawcett, 1988). Anatomical evidence obtained from amphibians has implicated the NMDA receptor in the activity-dependent process (Cline et al., 1987; Cline and Constantine-Paton, 1989). These data led to the hypothesis that one function of the NMDA receptor is as a detector of correlated afferent activity serving as the first step in a cascade of events that stabilizes inputs that are coactive (Cline and Constantine-Paton, 1989; Constantine-Paton, 1990). However, despite the wealth of data on the stimulus selectivity of retinal ganglion cells (RGCs) (Grusser and Grüsser-Cornehls, 1976; Ewert, 1984) and the ability of their terminals to reorganize following a wide variety of perturbations (for review, see Levine, 1984; Sharma and Romeskie, 1984; Udin and Fawcett, 1988), relatively little is known about the response properties and synaptic interactions of the tectal neurons themselves.

Attention has recently been focused on the responses and receptor physiology of tectal cells, as a result of a number of studies demonstrating that chronic application of DL-2-amino-5-phosphonovaleric acid (DL-APV), the blocker of the NMDA subtype of excitatory amino acid receptor, to the tectum can disrupt several characteristics of RGC synaptogenesis within the tectal neuropil. Specifically, map refinement, map registration, and ocular dominance segregation are disrupted by chronic DL-APV treatment (Cline et al., 1987; Cline and Constantine-Paton, 1989, 1990; Scherer and Udin, 1989; Schmidt, 1990). All of these properties of the mapping process are known to depend on normal temporal patterns of RGC action potential activity (Meyer, 1982; Reh and Constantine-Paton, 1985; Schmidt and Eisele, 1985), and a number of studies have now shown that proximity of the ganglion cell bodies in the retinal sheet is reflected in their activity patterns. Action potentials in

Received Jan. 4, 1993; revised Apr. 13, 1993; accepted Apr. 15, 1993.

We thank Dr. Thomas Carew, Dr. Haig Keshishian, and Dr. David McCormick for extensive comments and suggestions on experiments and an earlier draft of the manuscript. We also thank Dr. Mark Blanton for providing information on the whole-cell voltage-clamp procedure in the slice, and Dr. Charles Stevens for loan of equipment. This work was funded by NIH Grants EY 06039 (M.C.-P.) and EY 07115 (P.W.H.).

Correspondence should be addressed to Martha Constantine-Paton, Yale University Department of Biology, P.O. Box 6666, New Haven, CT 06511.

ganglion cells are temporally correlated only if their cell bodies lie in the same retinal locale (Arnett, 1978; Mastronarde, 1983a,b; Maffei and Galli-Resta, 1990; Meister et al., 1991). The demonstrated correlations in RGC activity and the effects of application of APV suggest that the activity-dependent mechanism that controls the local process of synaptogenesis during map development and regeneration may be similar in mechanism to the correlation-dependent increase in synaptic efficacy first proposed by Hebb (1949). A form of adult plasticity, also thought to follow Hebbian rules, is found in several brain regions and is known as associative long-term potentiation (LTP) (Bliss and Lomo, 1973). LTP is also known to be dependent on NMDA receptor activation in the CA1 region of hippocampus and in superficial layers of visual cortex (Artola and Singer, 1987; for review, see Brown et al., 1988). Thus, there may be similarities in the mechanisms underlying some forms of adult plasticity and developmental plasticity. However, more information on synaptic plasticity in developing systems is necessary to assess this possibility.

Earlier work on the pharmacology of tectal neurons has used extracellular techniques to demonstrate that the dominant optic tract neurotransmitter is likely to be an excitatory amino acid (Langdon and Freeman, 1986, 1987; Debski et al., 1987; Debski and Constantine-Paton, 1988), and that the postsynaptic component of the field potential evoked in the tectum by optic nerve stimulation has both APV-sensitive and APV-insensitive components (Debski and Constantine-Paton, 1988; Hickmott and Constantine-Paton, 1989). However, all work at the level of tectal single units has been concerned either with intracellularly recorded response properties such as latencies of EPSPs and IPSPs in response to electrical stimulation of the optic nerve (Matsumoto and Bando, 1980; Hardy et al., 1984, 1985; Antal et al., 1986; Leresche et al., 1986; Matsumoto et al., 1986), or with extracellularly recorded responses to visual stimulation of the retina and actions of broad classes of candidate transmitter agonists and antagonists (for review, see Freeman and Norden, 1984).

In order for the Hebbian model of NMDA receptor–dependent LTP to be unambiguously generalized to the retinotectal synaptic neuropil during development and regeneration, the majority of tectal neurons immediately postsynaptic to RGC inputs should express both NMDA and non-NMDA excitatory amino acid receptors. Furthermore, activation of RGC synapses on these neurons should generate substantial current flow through these channels. However, if a large proportion of normal retinotectal synaptic transmission is carried by the NMDA channel, then the interpretation of the effects of blocking the NMDA channel in the tectum would be complicated by this general block of synaptic transmission (for review, see Fields and Nelson, 1992). In the visual cortex, for example, it is known that several measures of developmental activity-dependent synaptic remodeling are blocked by procedures that simply prevent retinal stimulation from effectively activating cortical neurons (Shaw and Cynader, 1984; Stryker and Harris, 1986; Reiter and Stryker, 1988; Miller et al., 1989; Fox et al., 1991).

At present there is only indirect evidence that APV does not block retinal activation of tectal cells. A recent study in frog tecta chronically and acutely treated with DL-APV failed to find any evidence of decreased transmission in the subset of tectal neurons participating in the circuit from one tectal lobe to the other via the nucleus isthmi and driven by RGCs from the contralateral retina (Udin et al., 1992).

To examine the role of glutamatergic transmission at the level of single tectal neurons directly driven by retinal input, we developed an *in vitro* preparation in which brains of late larval and young postmetamorphic *Rana pipiens* frogs are cut such that each slice contains the diencephalic optic tract and the tectal termination of the RGC axons. These slices can be maintained *in vitro* for at least 8 hr (Hickmott and Constantine-Paton, 1989). The preparation has permitted whole-cell voltage-clamp analyses of tectal neurons with subsequent morphological identification of the physiologically studied cells. Here we report on receptor types and some of the membrane properties expressed by these neurons. We also examine the relative contributions to the synaptic current elicited in these neurons by NMDA and non-NMDA excitatory amino acid receptors in response to electrical stimulation of the optic tract.

Some of these results have appeared in abstract form (Hickmott and Constantine-Paton, 1990).

Materials and Methods

Rana pipiens tadpoles were raised from embryos in dilute Instant Ocean (0.5 gm/liter) on a 12/12 hr day/night cycle. Early tadpoles were fed powdered nettle, while later larval stages were fed boiled romaine lettuce. All staging followed Taylor and Kollros (1946). In some experiments, tadpoles of two closely related species, *Rana catesbiana* and *Rana utricularia*, were used with identical results.

Slice preparation. Tectal slices for physiology were obtained using a procedure modified from Cline and Constantine-Paton (1987). Late-stage (XVI–XXV+) tadpoles or postmetamorphic frogs were completely anesthetized in 0.1% ethyl *m*-aminobenzoate (MS 222; pH 7.4; Sigma). The brain was rapidly removed, and the dura and telencephalon were dissected from the brain. The brain was then immersed in solidifying low-gelling-temperature agar (Sigma type 7, 4.3%) at an angle, such that the trajectory of the optic tract through the diencephalon was parallel to the top of the block, which subsequently defined the plane of section. As soon as alignment was achieved, the brain in agar was placed in a freezer at −20°C for 90 sec, followed by a freezer at −70°C for 30 sec to harden the agar and cool the tissue. The block was then trimmed and mounted on a chilled brass chuck with Histoacryl blue glue (Trihawk International) or Vetbond (3M Corp.) and sectioned at 500 μm in a vibratome chamber (Oxford) filled with ice-cold, dextrose-supplemented bicarbonate buffer (in mM: NaCl, 112; KCl, 2; $NaHCO_3$, 17; $CaCl_2$, 3; $MgCl_2$, 3; dextrose, 12.2; pH 7.3–7.4). This was the same basic medium used in our recording chamber. Slices generally included a large proportion of the optic tract, as well as a strip of optic tectum containing the terminal arborizations of many of the RGC axons running parallel to the plane of the section (see Fig. 1*A*). The slice was secured to the bottom of a low-volume recording chamber by a solidified thrombin clot (see Blanton et al., 1989), and was further stabilized with a dot of Histoacryl blue glue or Vetbond at the corners of the agar surrounding the tissue. A vibration isolation table (Technical Manufacturing Corp.) was used to prevent vibration in the recording setup. The slice was maintained in cold bicarbonate-buffered saline (16–18°C), which was continuously bubbled with 95% O_2, 5% CO_2 and perfused over the slice at a rate of 1–2 ml/min. The slice chamber was mounted on the stage of a modified fixed-stage Leitz Laborlux microscope, and viewed under low power (40×) for the duration of the experiment. Even at this low power, the laminae of the tectum could be differentiated. Slices were allowed to equilibrate for at least 1 hr submerged in bicarbonate buffer before any attempt to record was made, as it was impossible to record stable potentials during this time.

Physiology. All currents were recorded with an Axopatch 1D amplifier (Axon Instruments) from neurons in layers 6 or 8 using the blind, single-electrode, whole-cell voltage-clamp method developed by Blanton et al. (1989). Membrane voltage was monitored on a separate channel of this amplifier and displayed on an analog oscilloscope (Tektronix model 5113). Currents were filtered with a Bessel low-pass filter at 2 kHz, digitized at 1–10 kHz, and stored on an Epson Equity II computer using a Rapidsystems Data Acquisition System (4×4), or on a Macintosh IICX computer using custom-written software for a Lab-NB acquisition board (National Instruments); currents were also monitored continuously on an oscilloscope.

Recording electrodes were pulled from soft glass (Drummond Scientific Co.) to a tip diameter of ~1.5–2 μm. For most voltage-clamp experiments, the electrode was filled with high-Cl^- solution (referred to subsequently as high-Cl^- solution) (in mM: CsCl, 100; EGTA, 10; HEPES, 20; $MgCl_2$, 3; tetraethylammonium chloride, 5; NaCl, 1; pH 7.2–7.3), yielding electrode resistances of 5–12 MΩ. This solution was used for two main reasons: (1) it yielded electrodes of lower resistance than other filling solutions used, and (2) it was easier to examine the overall polysynaptic contributions to the postsynaptic current (PSC), which are primarily mediated by Cl^--dependent inhibition, with the Cl^- reversal potential depolarized by high internal Cl^-. Instead of differentiating between inhibitory and excitatory contributions to the PSC, we could use a single measure (T_{half}; see below) to measure the overall effects of various antagonists on the polysynaptic region of the PSC. For experiments where we were interested in differentiating excitatory from inhibitory (Cl^--dependent) currents, a low-Cl^- filling solution was used, so that the reversal potential of Cl^--dependent currents would be markedly different from cationic-dependent currents. This solution, referred to as low-Cl^- solution, contained (in mM) Cs-methanesulfonate, 100; EGTA, 10; HEPES, 20; $MgCl_2$, 3; NaCl, 1; pH 7.2–7.3. These electrodes typically had resistances of 8–14 MΩ. These two filling solutions were also used for experiments where both current and voltage clamp were performed. In all cases, 2 mM Mg-ATP was also added to avoid possible washout of synaptic currents; also, 1–1.5% biocytin (Sigma) was included so that the morphology and position of recorded cells could be subsequently documented. Cs-based solutions were used to block K^+ currents, thus greatly increasing the control of membrane voltage. The electrode was roughly positioned in tectal layer 6–7 (Székely and Lázár, 1976), and slowly (0.5 μm/sec) advanced through the tissue using a motorized drive (model 860, Newport Instruments, Inc.). Slight positive pressure was applied through the electrode to prevent clogging. The current resulting from voltage pulses (+20 mV, 10 Hz) was continuously monitored on an oscilloscope, and when this current decreased (usually by 100–200 pA), gentle suction was applied through the electrode to form a gigaseal (typically >10 GΩ). After compensation for electrode capacitance, strong suction was used to rupture the membrane, giving access to the whole cell, as detected by an increase in the capacitative transients of the current, corresponding to the membrane capacitance of the cell. The membrane capacitance was compensated for, and the series resistance of the cell determined, and examined periodically throughout the experiment.

The resting potential of a cell was determined by varying the holding potential until zero current was detected. The approximate input resistance was determined using a −100 mV square pulse and measuring the resulting current at 300 msec latency to avoid factoring in capacitative currents. To avoid cells that were damaged or may have sealed to the electrode poorly, only cells with resting potential between −70 mV and −40 mV with input resistance of >0.25 GΩ were used.

PSPs and PSCs were evoked by electrical stimulation of the optic tract in the dorsal thalamus usually just before it penetrated the midbrain. Stimulating electrodes were bipolar, consisting of two polypropylene-insulated tungsten electrodes (0.9–1.1 MΩ; Micro Probe, Inc.) cemented to a glass pipette; their tips were drawn together with a hair and secured with wax for a final tip separation of 30–100 μm. To obtain relatively stable stimulating efficiencies and to protect the electrode tips, the exposed tungsten of the stimulating electrode was electrolytically plated first with gold and then with platinum. Stimulation was at 0.01 msec duration at sufficient voltage (60–90 V) to evoke a maximal PSC, and pulses were delivered at 20–40 sec intervals. To obtain monosynaptic currents, we used the minimal stimulus (10–38 V) necessary to evoke a visible response. Such currents were considered to be monosynaptic if they met two criteria: their latency (measured from the stimulus to the beginning of the PSC) was less than 8 msec, and they were unchanged after stimulation at 3 Hz for 5 sec. Eight milliseconds is a reasonable latency criterion based on the reported latency values of electrically evoked PSPs from frog tectum (Matsumoto and Bando, 1980), the Q_{10} values determined for conduction velocity and synapse delay for frog neuromuscular transmission (Katz and Miledi, 1965), and the temperature of our slices (16–18°C). These data yield approximate minimum latency values for monosynaptic EPSPs in adult frogs ranging from 2.5 to 7.5 msec. For each PSC, a current–voltage (I–V) relation and reversal potential was determined by examining the peak PSC amplitude at various holding potentials (V_{hold}), usually −80 to +20 mV.

Pharmacology. To examine the relative contributions of various transmitter receptor systems to the synaptic current evoked by optic tract stimulation, antagonists of the (*R,S*)-α-amino-3-hydroxy-5-methylisoxazole-4-propionic acid (AMPA), the NMDA, or the $GABA_A$ receptor were added to the basic buffer solution. All drugs were dissolved in bicarbonate buffer and bath-applied via gravity-fed perfusion at a rate of 0.5–1.5 ml/min. Drugs used were the NMDA receptor antagonist DL-APV (80–100 μM), the AMPA receptor antagonist 6-cyano-7-nitroquinoxaline-2,3-dione (CNQX) (5–10 μM), and the $GABA_A$ antagonist (−)bicuculline methiodide (BMI) (20–40 μM). In some experiments where maximal NMDA receptor activation was desired, a "low-Mg" buffer containing 0.5 mM or 0 mM $MgCl_2$ instead of the normal 3 mM $MgCl_2$ was used.

In all of these experiments, prior to changing the bathing solution, the membrane potential of the cell was held near the resting potential and the stimulating voltage was increased until a maximal PSP or PSC was obtained. Five control PSCs were gathered and subsequently averaged. The experimental solution was then washed into the slice chamber for 10–15 min, which was the incubation time required for a maximal drug response. Five PSPs/PSCs evoked in this solution were stored and averaged to yield the treated response. Washout of the drug was achieved by bathing with normal bicarbonate buffer for 15–30 min. If the cell response was still within 10–20% of the original amplitude, another antagonist was applied using the same procedure.

Plots of the averaged PSCs (control, treated, and washout) were obtained and subsequently analyzed to determine the amplitude at the short-latency peak of the PSC (A_{peak}). The time required for the PSC to fall to half of this peak amplitude (T_{half}) was also measured to obtain a quantitative index of the contribution of longer-latency components to the postsynaptic response. Values of A_{peak} and T_{half} without drug treatment for all experiments were obtained by averaging the A_{peak} and T_{half} values for the control and washout plots associated with the particular drug application. The A_{peak} or T_{half} value obtained during the particular drug treatment was then divided by this average to determine the percentage change in the presence of the drug. All data are expressed as mean ± SEM and were analyzed using Student's t test.

Agonist iontophoresis. In some slices, iontophoresis of agonists was used instead of electrical stimulation to evoke PSCs in tectal neurons. In these slices, all synaptic transmission was blocked with 0.5–1.0 μM of the sodium channel blocker tetrodotoxin (TTX), thus isolating the cell from any action potential–evoked synaptic inputs. Iontophoresis electrodes were pulled from four-barrel filament glass (AM Systems), the tip of which was broken back under a microscope to approximately 4–5 μm. Each barrel was then filled with one of three agonists at a concentration of 50 mM (pH 7–7.5): AMPA-HBr, NMDA, or GABA. The fourth barrel was filled with 50 mM NaCl and served as a current balance channel. The electrode was then connected to an iontophoresis device (Neuro Data Instruments, model IP-X5) and lowered into the saline, and the tip resistance of each barrel was determined using a +1000 nA, 1 sec pulse. Tip resistances ranged from 20 to 100 MΩ, and tended to be similar among the four barrels. A small (50–100 nA) retaining current was continuously applied to each barrel. After a stable recording was obtained, the iontophoresis electrode was advanced into the tissue under visual control until its tip appeared to be near the recording electrode tip. Large (−1000 nA, 1-sec-duration) current pulses were then applied to the AMPA barrel to determine if the neuron under whole-cell clamp showed a response; the iontophoretic electrode was subsequently moved to optimize this response. At this point, the ejection current was increased or decreased for each agonist such that a maximal response to each was obtained. The agonist-evoked currents were elicited at a variety of holding potentials, and a current–voltage plot was obtained for each. At least 90 sec were allowed to pass between each agonist application.

Histology. During the recordings, biocytin present in the recording electrode diffused into the neuron. In most cases, to facilitate this process, −20 mV, 100 Hz pulses were given for 5–10 min at the end of the recording. Filled neurons could then be visualized using an avidin reaction (Horikama and Armstrong, 1988). During the recording session the approximate position of each neuron from which a particular set of physiological data was obtained was noted by recording its position in the slice using an eyepiece grid. After the 8–12 hr recording sessions, slices were fixed overnight at 4°C in 4% paraformaldehyde in phosphate-buffered saline (PBS). They were then rinsed in several changes of PBS for at least 1 hr and resectioned at 80–100 μm on a vibratome. These sections were immersed in 0.5% H_2O_2 for 20 min to saturate endogenous peroxidases and then rinsed for 40 min. They were subsequently incubated for 90 min in 0.0025% peroxidase-conjugated avidin (Sigma)

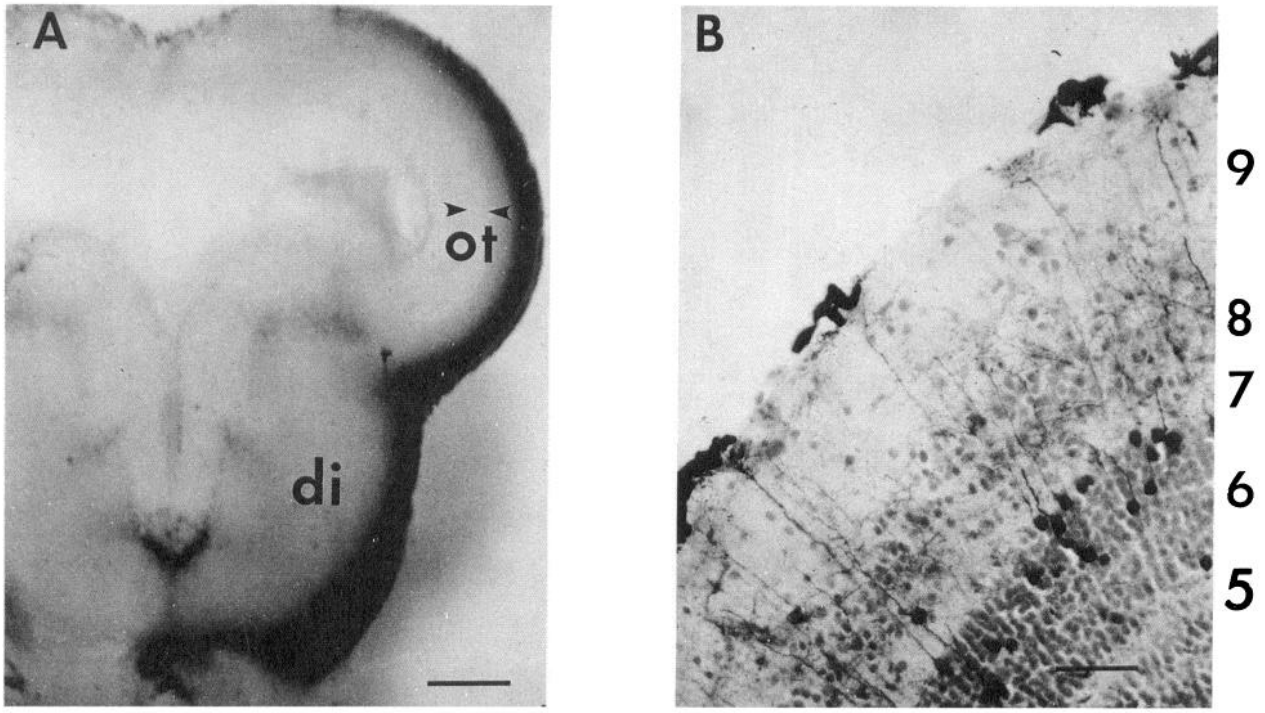

Figure 1. Anatomy of the tectal slice. *A,* An example of a tectal slice from a *Rana pipiens* tadpole. Before slicing, the entire optic nerve was labeled with HRP, and subsequently reacted with DAB to yield a dark reaction product. The reaction product was seen in the optic tract as it runs along the diencephalon (*di*), and also in the termination zone of the optic terminals in the optic tectum (*ot*). The *arrowheads* approximately delimit tectal layer 6, which is the primary cellular layer of the tectum and contains neurons immediately postsynaptic to the optic tract, and where most of the cells examined in this study were. *B,* A cross section of the optic tectum from a young postmetamorphic frog, showing cellular architecture. Cresyl violet staining revealed the alternating plexiform (5, 7, 9) and cellular (6, 8) layers. Layers 1–5 contained cells and fiber tracts concerned primarily with multimodal inputs (Lázár, 1984), and were not examined in this study. In this animal, HRP was injected into a tectal efferent zone near the nucleus isthmi. Projection neurons in the tectum were thus retrogradely labeled with HRP (dark reaction product). For further details concerning this figure, see Law and Constantine-Paton (1982). Scale bars: *A*, ~400 μm; *B*, 200 μm.

in PBS containing 0.25% Triton X-100, and rinsed for at least 60 min in several changes of PBS. This was followed by an additional 30 min wash in Tris-buffered saline (TBS: 0.58 gm NaCl in 100 ml of 50 mM Tris, pH 7.4). HRP-labeled neurons were visualized by incubating the sections in 0.05% 3,3′-diaminobenzidine tetrahydrochloride (DAB) in TBS for 20 min, and reacting them in 0.05% DAB in TBS with 0.006% H_2O_2 and 0.015% dimethyl sulfoxide for 2 min. For microscopy the sections were rinsed in PBS for 1 hr and mounted on slides in 80% glycerol.

Sections containing labeled neurons were examined on a Leitz Dialux microscope and individual cells were reconstructed using a 63× oil-immersion objective and a camera lucida attachment. Neurons were photographed using a Nikon FE2 35 mm camera and a 20× objective with Kodak Technical-Pan film. In some early experiments, FITC-conjugated avidin was used instead of the peroxidase-conjugated avidin. In these cases the sections could be viewed shortly after fixation, washing, and mounting in 80% glycerol with 20 mM *n*-propylgallate. Neurons labeled with FITC were examined using epifluorescence for fluorescein, and drawn using the camera lucida system described above. Photography was the same as described above for peroxidase-labeled neurons.

Results

General. The main objective of this study was to determine the contribution of different amino acid transmitter receptor systems to tectal neuron responsiveness at the developmental stages where effects of chronic drug treatment have been observed on RGC terminals. Consequently, all slices were taken from late-stage tadpoles or young frogs within 2 weeks of metamorphosis. There were no systematic differences in data obtained from younger versus older animals, so data were pooled across stages.

In amphibians, RGC axons constitute the dominant input to the superficial tectal neuropil (Fig. 1*A*). The optic tectum itself is a highly ordered laminar structure consisting of nine cellular and plexiform layers (Fig. 1*B*). Layer 9, the most superficial, contains the various classes of RGC afferents as well as the dendritic arborizations of the tectal neurons lying in layers 8 and 6. Layer 8 is a sparse cellular layer that contains most of the large ganglionic cells driven by the retina. Layer 7 is the primary efferent layer. Layer 6 is the cellular layer containing most of the visually driven cells. The deeper tectal layers are primarily concerned with nonvisual and multimodal inputs and were not examined in this study (Székely and Lázár, 1976). All neurons examined had their somata in layers 6 or 8 with the majority occurring in layer 6.

Extracellular recordings (Hickmott and Constantine-Paton, 1989) indicate that tectal slices are viable for >12 hr. However, it typically becomes progressively more difficult to obtain good gigaseals on neurons as time progresses. Therefore, all recordings in this study were made between 1.5 and 10 hr after preparing the slice. Since most tectal neurons are small (<10 μm) and fragile, we decided to use whole-cell voltage clamp rather than standard intracellular recording. This yielded higher signal-to-noise ratios and more stable recordings. Even so, many cells could be held for only a short period of time (<10 min). This was sufficient for determining resting potential and input resistance. Resting potential was determined for 71 cells and ranged from −40 to −70 mV (mean = −49.8 ± 0.76 mV). This wide range probably reflects several variables, including replacement of K^+ inside the cell with Cs^+ from the electrode. Input resis-

tance was determined for 38 cells and ranged from 0.5 to 10 GΩ (mean = 3.5 ± 0.17 GΩ). Within these groups there was no tendency for cells with lower resting potential or lower input resistances to be less stable, as might be expected if the lower values were indicative of severely damaged or dying cells.

The mean series resistance of tectal neurons was 22.1 ± 1.5 MΩ and ranged from 12 to 46 MΩ; the mean membrane capacitance was 2.54 ± 0.24 pF and ranged from 0.5 to 5.4 pF. The average time constant of the membrane, calculated using these parameters, was 59.54 ± 9.16 μsec. Since the synaptic currents we examined have much slower kinetics than this time constant, our currents are not significantly contaminated by capacitative currents. Since most tectal neurons have small somata and fine but extensive dendritic arbors, and all of our patches were on cell somata, it is unlikely that the membrane voltage over the entire cell could be closely controlled by the electrode. Indeed, depolarizing voltage steps in many cells resulted in large, rapid, short-duration currents that reflect action potential activity (as seen in current clamp), and other uncontrolled voltage-activated currents. Furthermore, these "spike currents" could also be found superimposed on electrically evoked PSCs, again reflecting spike activity seen in current clamp. These spike-related events were never seen in the presence of 0.5–1.0 μM TTX. While we were unable to control these rapid, large events, there was sufficient voltage control to resolve slower synaptically activated currents, and to determine reversal potentials successfully. Furthermore, current-clamp recording was used to verify that the conductances we examined represented PSCs underlying PSPs. All the pharmacological data presented for PSCs were qualitatively identical with those determined for PSPs recorded under current clamp.

Spontaneous synaptic currents. The first evidence of PSCs in all neurons examined was the presence of frequent, relatively small currents, probably reflecting both spontaneous release of transmitter and spontaneous spikes in afferent synapses. When the neurons were held at their resting potentials the spontaneous currents ranged from 10–50 pA. Using the standard, CsCl-based filling solution (high-Cl^- solution), these spontaneous currents were inward at resting potential, but they could be reversed by holding at more depolarized potentials. The V_{rev} of all spontaneous currents carefully examined was approximately the same as the V_{rev} for the synaptic currents evoked by electrical stimulation of the optic tract in the same cell ($n = 8$ neurons). Using low-Cl^- solution, both spontaneous excitatory PSCs (EPSCs) and inhibitory PSCs (IPSCs) could be resolved by their difference in reversal potential, which was about −10 to +5 mV for EPSCs and −55 to −45 mV for IPSCs (data not shown). IPSCs tended to have larger amplitudes than EPSCs.

Monosynaptic currents. Since we are particularly interested in the possible role of the NMDA receptor in the development of the retinotopic map, we began by examining the characteristics of the direct retinotectal synapses. Thus, we examined putative monosynaptically activated currents by using our two criteria (latency of <8 msec and ability to follow stimuli at 3 Hz) and minimal stimulation. All such recordings were made using low-Cl^- solution in the pipette and in the presence of 3 mM Mg^{2+} in the bath. Using this minimal stimulation paradigm, we recorded monosynaptic currents from 15 cells. The mean reversal potential, measured at the peak of this short-latency EPSC, was −4.5 ± 2.13 mV, which agrees closely with the value obtained for the short-latency polysynaptic EPSC obtained using maximal stimulation (see below).

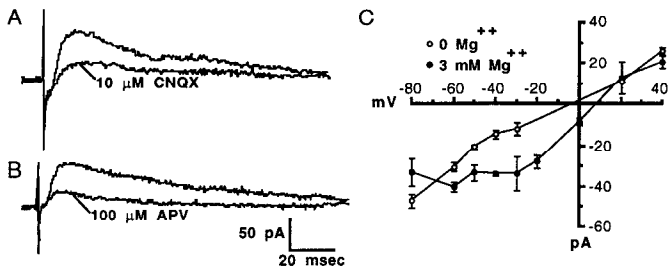

Figure 2. Effects of glutamatergic antagonists CNQX and DL-APV on monosynaptic EPSCs evoked by minimal electrical stimulation, and recorded using low-Cl^- solution in the pipette. All neurons were held at +20 mV to eliminate Mg^{2+} block of the NMDA receptor channel. Each trace is the average of five individual EPSCs. The early, rapid outward/inward currents represent stimulus artifacts. *A,* Effects of the non-NMDA glutamate receptor antagonist CNQX (10 μM) on the monosynaptic PSC. In all cases (five of five), CNQX reversibly decreased the EPSC, as illustrated here. *B,* Effects of the NMDA receptor antagonist DL-APV (100 μM) on the monosynaptic EPSC. In most cases (five of six), DL-APV also reversibly reduced the PSC. In one cell, DL-APV had no effect. *C,* Current–voltage plots for monosynaptic EPSCs recorded from the same cell in the presence (*solid circles*) or absence (*open circles*) of 3 mM Mg^{2+}. Each point represents the average of three individual EPSCs evoked from a single cell at the indicated holding potential, and the error bars represent the SEM. Values were all measured at 8 msec after the stimulus. Note the voltage dependence of the plot in the presence of Mg^{2+} (*solid circles*) in the region of −60 to −20 mV, which probably reflects the voltage-dependent block of the NMDA channel by external Mg^{2+}. In the absence of Mg^{2+} (*open circles*), this voltage dependence is eliminated.

Pharmacological evidence supports the presence of both non-NMDA-mediated and NMDA-mediated currents in these monosynaptic EPSCs. We examined the effects of bath-applied CNQX and DL-APV on monosynaptic currents from neurons that were held at +20 mV to be sure that the Mg^{2+} block of the NMDA channel was completely relieved. In all cases (five of five), CNQX considerably reduced the monosynaptic current (Fig. 2*A*). Additionally, in three of three cases where the neuron was held at −60 mV, CNQX completely eliminated the EPSC (not shown). As illustrated in Figure 2*B,* DL-APV also reduced the monosynaptic EPSC in four of five cases where the cell was held at +20 mV. When cells were held at −60 mV, DL-APV reduced the EPSC only slightly in one of five cases, reflecting a blockade by Mg^{2+} of the NMDA current at hyperpolarized potentials.

The *I–V* curves of many of these monosynaptic EPSCs also suggested the presence of an NMDA receptor–mediated current. In the presence of 3 mM Mg^{2+}, 9 of 13 of these *I–V* curves showed a region of voltage dependence between −60 to −20 mV (Fig. 2*C,* solid circles). This region is not observed in the absence of external Mg^{2+} (Fig. 2*C,* open circles). These characteristics suggest that the voltage dependence reflects the negative slope conductance of the NMDA channel detected in high Mg^{2+} in other systems (Mayer et al., 1984; Mayer and Westbrook, 1987; Hestrin et al., 1990a).

Currents evoked by maximal stimulation. Stable PSCs were evoked by maximal optic tract stimulation in 55 neurons, using the high-Cl^- solution in the recording electrode. An example of an average of such PSCs at two different holding potentials (−60 and +40 mV) is shown in Figure 3*A*. The PSCs in these tectal cells generally consisted of a short-latency, large-amplitude current (open arrowhead) with a long-latency tail (solid arrowhead). Repetitive stimulation of the optic tract (1–5 Hz) invariably

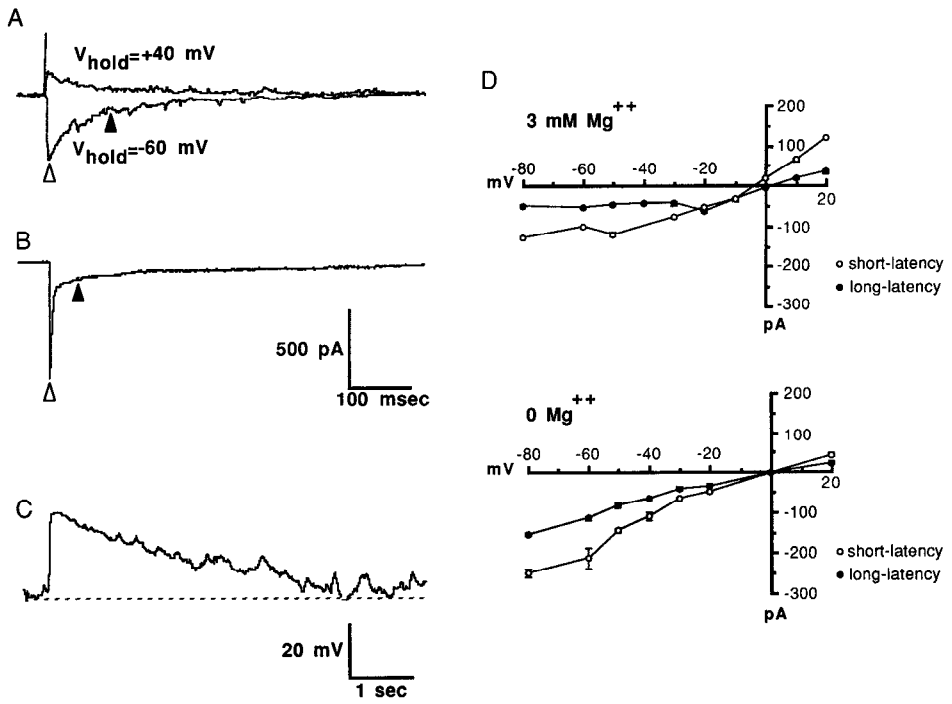

Figure 3. Examples of electrically evoked responses in tectal neurons using maximal stimulation of the optic tract. Each trace is the average of five individually evoked PSCs (*A, B*) or PSPs (*C*). *A,* Representative examples of an averaged, evoked PSC held at −60 mV (inward current) and at +40 mV (outward current), showing reversal of the PSC (V_{rev} ~ 0 mV). The cell was recorded using high-Cl^- solution in the pipette, and was bathed in medium containing 3 mM Mg^{2+}. The *open arrowhead* indicates the point at which the short-latency component (A_{peak}; Table 1) was measured, while the *solid arrowhead* indicates the point at which the long-latency component (T_{half}; Table 1) was measured. The small, brief inward currents in the *lower trace* represent spontaneous currents that have not been completely averaged out. The very rapid, early outward current is the stimulus artifact. *B,* Representative example of an averaged, electrically evoked PSC recorded using low-Cl^- solution in the pipette so that EPSCs and IPSCs could be differentiated by differing reversal potential. The cell was held at −60 mV. The *open arrowhead* again indicates the short-latency component (primarily EPSCs) and the *solid arrowhead* indicates the long-latency component (a combination of EPSCs and IPSCs, dominated by IPSCs). *C,* A representative average of electrically evoked PSPs recorded using high-Cl^- solution. The resting potential of the neuron was −52 mV. Note that, as illustrated in Figure 2*A* for the evoked PSC, there was both a short-latency component and a longer-latency component. As in *A,* even though the trace represents an average, there was evidence of large, spontaneous events. Note the change in scale from *A* and *B. D,* Current–voltage plots for a tectal neuron in 3 mM Mg^{2+} (*top*) and 0 mM Mg^{2+} (*bottom*) bathing medium. The *open circles* were measured at the short-latency peak of the PSC (A_{peak}), while the *solid circles* were measured at 100 msec after the stimulus (T_{half}), and reflect the long-latency component. Each point represents the average of currents measured in the same cell in response to three separate stimulations of the tract. The error bars represent the SEM.

produced a decrease in the long-latency tail of these PSCs, while showing little or no effect on the short-latency peak (data not shown). This suggests that the short-latency peak most closely reflects a summation of monosynaptic inputs from the optic tract, while polysynaptic inputs contribute substantially to the long-latency components of the PSC. However, even during high-frequency stimulation, a variable amount of the long-latency current remained. Thus, slow and delayed monosynaptic currents probably contribute to the long-latency portions of the PSC also. Such currents could reflect the slow kinetics of the NMDA current, or other slow currents, such as those produced by peptide transmitters known to be localized in some RGC terminals (Kuljis et al., 1984). Nevertheless, the long-latency component of the response is enriched in polysynaptic responses compared to the short-latency component. In a few cases, we compared the effects of stimulating at 1–5 Hz before and during DL-APV treatment; DL-APV blocked a portion of the current that was unable to follow this high-frequency stimulation (data not shown), indicating that at least some of the effect of DL-APV is definitely on polysynaptic currents. This does not, however, rule out an effect of DL-APV on monosynaptic currents.

To dissect better the inputs contributing to these PSCs, we used low-Cl^- recording solution and maximal stimulation of the tract to obtain currents from 20 neurons (Fig. 3*B*). In each of these, the PSC was clearly divided into an early monosynaptic EPSC (open arrowhead), followed by a longer-latency, predominantly polysynaptic current. Based on the low amplitude of the latter component compared to currents with comparable latency measured with the high-Cl^- electrode solution, the long-latency component was probably a combination of IPSCs and EPSCs.

To examine synaptic responses to electrical stimulation under more physiological membrane potentials, we examined PSPs evoked with maximal stimulation of the tract in five neurons using current clamp and the high-Cl^- pipette solution (Fig. 3*C*). These PSPs closely resembled the PSCs, except they had a longer duration, probably reflecting prolongation of the underlying current due to the cable properties of the neuron. In six cells where the low-Cl^- pipette solution was used, PSPs elicited by maximal stimulation exhibited an EPSP/IPSP combination similar to those seen for PSCs under the same conditions.

We compared these currents in normal bathing medium and in bathing medium in which there was no added Mg^{2+}. Figure 3*D* shows representative *I–V* plots of both the short-latency, primarily monosynaptic component (A_{peak}), and the long-latency

tail (T_{half}) in the presence (top) and absence (bottom) of Mg^{2+}, using the high-Cl^- pipette solution (see Materials and Methods for definitions of A_{peak} and T_{half}). Note that for both the short- and long-latency components there is a pronounced voltage dependence in the region of −60 to −20 mV. This voltage dependence is not seen when external Mg^{2+} is removed, suggesting that it reflects the negative slope conductance of the NMDA channel detected in high Mg^{2+} (Mayer et al., 1984; Mayer and Westbrook, 1987; Hestrin et al., 1990a). These observations are consistent with the pharmacological data (see Figs. 2, 4, 6) that indicate there is an NMDA receptor–mediated contribution to monosynaptic, as well as predominantly polysynaptic, components of tectal cell responses to optic tract stimulation.

Using the high-Cl^- pipette solution, the membrane holding potentials at which these electrically elicited currents reversed were determined for the same 55 neurons. These values, measured at the peak of the PSC, ranged from −40 mV to 10 mV for different neurons with a mean of −13.5 ± 2.8 mV. This is considerably different from the expected V_{rev} (~0 mV) for pure glutamate-activated currents (Crunelli et al., 1984; Mayer and Westbrook, 1987). Some of this discrepancy may be accounted for by our inability to clamp the membrane potential effectively in the dendrites, where the majority of synaptic currents actually arise (Hestrin et al., 1990b). However, it is also likely that the internal ionic concentration of these small neurons is abnormal, since the electrode, and hence the cell cytoplasm, contained high concentrations of Cl^- ions. Thus, the inhibitory drive to these cells may actually contribute to an apparently inward synaptic current, making the reversal potential appear more hyperpolarized than it would be if only cation channels were involved. Indeed, using the low-Cl^- pipette solution, which more closely reflects a normal internal milieu, the reversal potential for the short-latency peak of the PSC was more depolarized, with a mean of −4.25 ± 1.82 mV (n = 20 neurons). This value is not significantly different from the value determined for monosynaptic EPSCs (see above). The reversal potential of the late, polysynaptic region of the PSC was −40.8 ± 1.8 mV, reflecting the predominance of inhibition in this region of the PSC.

The presence of non-NMDA, NMDA, and GABA receptor–mediated currents in PSPs elicited by maximal stimulation of the tract was confirmed using current-clamp recording and bath application of antagonists specific to each of these neurotransmitter types (5–10 μM CNQX, 100 μM DL-APV, and 40–50 μM BMI). Figure 4 shows representative effects of these three antagonists on PSPs recorded using high-Cl^- solution and maximal stimulation. Figure 4*A* shows the effects of CNQX on an average of five such PSPs. In six of seven cells, CNQX reduced both the early and late components of the PSP. This reflects block of non-NMDA-mediated synaptic transmission at both monosynaptic, retinotectal synapses, as well as polysynaptic synapses responsible for the later components of the PSP (EPSPs and IPSPs). Figure 4*B* shows the effects of DL-APV on an averaged PSP; in five of six cases, DL-APV reduced the late portion of the PSPs, while having a smaller effect on the early portion. In one case, DL-APV caused an increase in PSP amplitude (not shown). These effects indicate that NMDA receptors are involved in both mono- and polysynaptic transmission, but that under conditions where the membrane voltage is not controlled they contribute more to polysynaptic and other long-latency events.

Data obtained using the low-Cl^- pipette solution (see Fig. 3*B*) implied that a large proportion of the polysynaptic component

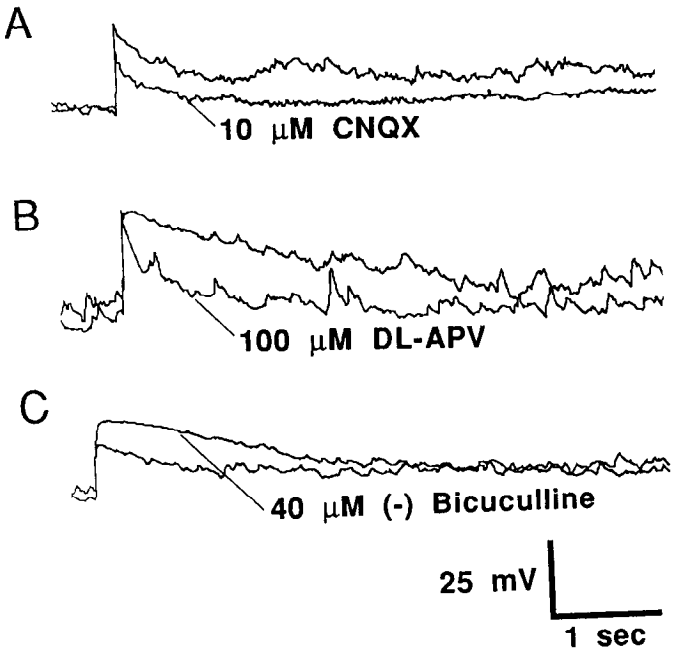

Figure 4. Examples of the effects of CNQX, DL-APV, and BMI on PSPs evoked using maximal stimulation of the optic tract and high-Cl^- pipette solution. As in Figures 2 and 3, each trace represents the average of five individual PSPs. All PSPs were recorded at the resting potential of the neuron and in 0 Mg^{2+} bathing saline. *A*, The effects of 10 μM CNQX on an averaged PSP recorded at the cell's resting potential (−59 mV). CNQX reduced both the early and late components of the PSP (see also Figs. 5, 6*A*; Table 1). *B*, Effects of 100 μM DL-APV on an averaged PSP recorded at the cell's resting potential (−52 mV). In contrast to CNQX, DL-APV reduced the late component of the PSP with no effect on the early component (see also Figs. 5, 6*C*; Table 1). The small positive deflections reflect the robust spontaneous activity in this neuron. *C*, Effects of 40 μM BMI on an averaged PSP recorded at the cell's resting potential (−51 mV). BMI substantially increased both the early and the late components of the PSP, probably reflecting a block of shunting inhibition.

of the tectal neurons' responses consisted of inhibitory events. This idea was supported by the effect of bath application of BMI on PSPs (Fig. 4*C*). In four of four cases, BMI increased the amplitude and duration of the PSP, particularly the late component, which contains the polysynaptic responses. This increase probably reflects a block of inhibition by the late IPSP. That BMI can also affect the early component implies that there may be tonic inhibition acting on some of the neurons in the tectum. Thus, blocking inhibition with BMI would tonically increase the resistance of the neuron, increasing the amplitude of the EPSP.

We also examined the effects of the three antagonists on PSCs evoked by maximal stimulation of the optic tract. PSCs yielded data that was consistently more stable, with a higher signal-to-noise ratio, and thus was used for quantitative analyses of the response. Bath application of at least one antagonist was successful (i.e., with good washout) for 35 tectal neurons, using maximal stimulation of the tract and the high-Cl^- pipette solution. In all cases the effects on the PSCs were similar to the data obtained from antagonist application on PSPs. Additionally, similar results were obtained using bath application of these antagonists and low-Cl^- pipette solution.

The data from these experiments are summarized in Table 1 and Figure 5, and examples of antagonist effects on the averaged

Table 1. Effects of antagonists on electrically evoked PSCs

		CNQX (n = 12 neurons)	DL-APV (n = 15 neurons)	BMI (n = 9 neurons)
Control	A_{peak}	296.6 ± 97.5	307.1 ± 83.1	237.3 ± 95.2
	T_{half}	141.3 ± 29.5	156.7 ± 2.5	138 ± 30.1
+ Antagonist	A_{peak}	144.0 ± 50.9*	311.9 ± 94.7	261.0 ± 104.4
	T_{half}	110.3 ± 28.5	85.3 ± 15.7**	1602 ± 256***
Fraction (antag/control)	A_{peak}	0.44 ± 0.07††	1.04 ± 0.15	1.12 ± 0.13
	T_{half}	0.77 ± 0.09†	0.55 ± 0.06	15.84 ± 3.49†††

Values are given as means ± SEM; n is the number of neurons examined that were successfully treated with the indicated antagonist. A_{peak} is defined as the amplitude (in pA) of the current from baseline to the peak of the short-latency component of the PSC. T_{half} is defined as the amount of time (in msec) from the start of the PSC to the time at which the PSC has decayed to 50% of A_{peak}. Control values represent the average of traces from before drug application and after washout. The fraction is the value during drug treatment divided by the appropriate control value.

* $p < 0.01$ compared with appropriate control.

** $p < 0.005$ compared with appropriate control.

*** $p < 0.0005$ compared with appropriate control.

† $p < 0.05$ compared with T_{half} fraction for DL-APV.

†† $p < 0.005$ compared with A_{peak} fraction of DL-APV or BMI.

††† $p < 0.0005$ compared with T_{half} fraction for DL-APV or CNQX.

PSCs are shown in Figure 6. Table 1 shows the effects of the three antagonists on A_{peak}, T_{half} (see Materials and Methods for definitions), and also the percentage response in the presence of drug (%) averaged over all neurons tested. Figure 5 graphs the percentage of cells responding to each of the three antagonists; a greater than 20% change in the indicated parameter (either A_{peak} or T_{half}) in response to drug treatment was used as a criterion for whether the cell responded or not. Twenty percent was chosen arbitrarily before any analysis was performed.

Examples of the differing effects of the three antagonists on PSCs are shown in Figure 6. Bath application of CNQX (Fig. 6*A*) significantly decreased the short-latency component (A_{peak}; Table 1) of PSCs (11 of 12 cells), while causing a smaller, but still significant, decrease in the longer-latency components in 6 of 12 cells (T_{half}; see Table 1). In addition, one neuron of the 13 tested had its entire PSC blocked by CNQX (Fig. 6*B*). These two observations suggest that CNQX directly blocks some retinotectal transmission, and also blocks some polysynaptic transmission.

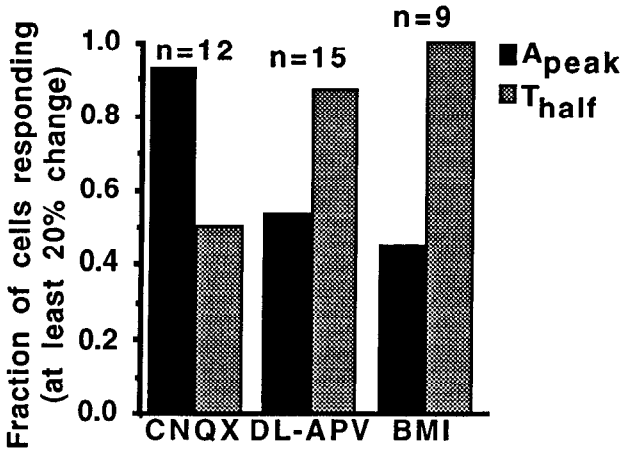

Figure 5. Histogram summarizing the effects of bath application of DL-APV, CNQX, and BMI on averaged PSCs recorded using high-Cl^- solution in the pipette (see also Table 1). Each *bar* represents the percentage of the total number of neurons that responded to each particular antagonist; n equals the number of cells tested for each antagonist. A neuron was considered to have responded if drug application caused at least a 20% change in either A_{peak} (*black bars*) or T_{half} (*gray bars*).

In contrast to CNQX application, bath application of DL-APV reversibly decreased the amplitude of the later components of the PSC (T_{half}), without significantly affecting the amplitude of the short-latency peak (A_{peak}) in 11 of 15 cells (see Table 1). This effect on a typical averaged PSC is shown in Figure 6*C*. In a few cells (3 of 15), DL-APV application caused an apparent increase in the excitability of the neuron, which manifested as an increase in the amplitude of the early component of the PSC with a normal reduction in the late component (data not shown). This observation suggested that some tectal cells were normally somewhat inhibited by NMDA receptor–bearing interneurons driven by optic tract input, as has been postulated previously (Debski et al., 1991; Udin et al., 1992).

The extent of optic tract–driven inhibitory input superimposed on the EPSCs in response to maximal tract stimulation was examined by bath-applying BMI. In all cases (nine of nine), BMI reversibly increased the duration of the PSC by a very large amount (reflected in an average 15.80× increase in T_{half}; see Table 1). In a few (four of nine) neurons BMI application also increased A_{peak} slightly, suggesting that inhibitory input can be active during both short- and long-latency components of the PSC.

Agonist iontophoresis. To confirm that non-NMDA, NMDA, and GABA receptors were definitely located on the postsynaptic cell from which we were recording, we examined the effects of iontophoretic application of exogenous agonists to these three receptors (GABA, NMDA, and AMPA, respectively) to neurons in tectal slices where 0.5 μM TTX was added to the bathing medium. In 9 of the 12 neurons tested, iontophoretic application of all three agonists—AMPA, NMDA, and GABA—had an effect on the neuron, typically a large, sustained current (Fig. 7*A*). In 2 of 12 cases NMDA had no effect, and in 1 of 12 cases GABA had no effect. These cases did not appear to result from clogged stimulating electrodes, and reflect the heterogeneity of the responses of tectal cells, as was seen using bath application

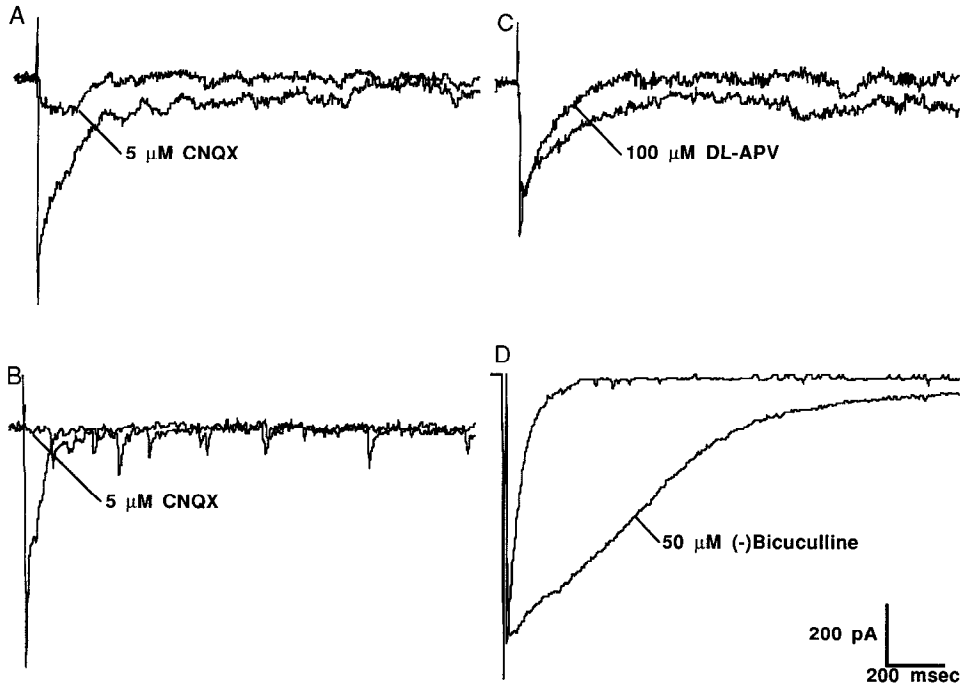

Figure 6. Examples of the effects of CNQX, DL-APV, and BMI on maximal electrically evoked PSCs recorded using the high-Cl^- solution in the pipette (for comparison to PSPs, see Fig. 4). There was also 3 mM Mg^{2+} in the bathing solution. Each trace represents the average of five individual PSCs. The rapid currents just before the PSC are stimulus artifacts. *A,* Representative effects of CNQX on the averaged PSCs. CNQX caused a reduction of the short-latency component coupled with a smaller reduction in the long-latency component. In the response shown, the control PSCs exhibited an unclamped spike current at the peak of the short-latency component. CNQX prevented this spiking. This cell was held at −60 mV. *B,* In one cell, CNQX caused a complete block of the PSC. Note that there were still spontaneous currents (probably IPSCs) present during the CNQX block. This cell was a layer 8 large ganglionic neuron, which was held at −80 mV. *C,* Effects of DL-APV on the PSCs. DL-APV decreased the long-latency component, without affecting the short-latency component. These PSCs were recorded from the same cell under the same conditions (held at −60 mV) as *A. D,* Representative effects of BMI on the PSCs. BMI greatly increased the long-latency component, and thus the duration of the PSC. This PSC was recorded from a layer 8 large ganglionic neuron, which was held at −40 mV.

of antagonist (see Fig. 5). At hyperpolarized holding potentials, GABA caused an outward current, while AMPA and NMDA caused inward currents. Nevertheless, examination of the *I–V* plots for AMPA and NMDA in the presence of 3 mM Mg^{2+} (Fig. 7*B*) revealed that only the NMDA-evoked currents exhibited a region of voltage dependence, corresponding to the region of negative slope conductance that is characteristic of NMDA-mediated currents in other neurons. This voltage dependence of the NMDA-evoked current was lost in 0 Mg^{2+} (Hickmott and Constantine-Paton, 1991). In addition, AMPA-induced currents could be blocked by 6 μM CNQX, but were unaffected by 100 μM APV, while NMDA-induced currents were blocked by 100 μM APV, but unaffected by 6 μM CNQX (Hickmott and Constantine-Paton, 1991).

Cellular morphology. Thirty neurons were recovered for morphological identification. All were found in layers 6–8, and the majority of these neurons (22 of 30) were small (soma diameter of 8–15 μm) pyriform cells located in layer 6 (Fig. 8*A,C*). These are the most common neurons in the optic tectum (Székely and Lázár, 1976). In addition to their small pear-shaped somata, these cells are characterized by a single apical process extending toward the surface that branched, sometimes profusely, in layers 8 and 9. Occasionally one or two small basal processes extended from the soma of these cells. The next most common neuronal type recovered (6 of 30) were large ganglionic neurons that lay in the superficial region of layer 6, or in layer 7 or 8 (Fig. 8*E*). These cells had larger somata (20–40 μm) and extended several long processes with a more tangential orientation up through

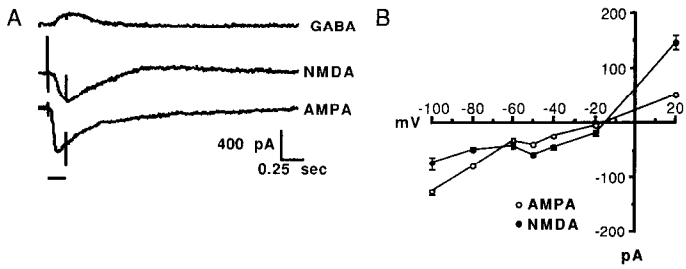

Figure 7. Examples of currents and the associated current–voltage plot evoked by the agonists GABA, NMDA, and AMPA in neurons bathed in 0.5 μM TTX. *A,* Each trace is the average of three agonist-evoked PSCs. The *bar* indicates the duration of the current (−1000 nA) activating the release of agonist; the large, rapid inward and outward currents at the *beginning* and *end of the bar* represent stimulus artifacts. Note that the time scale differs from that of the previous figures. These were all recorded from a layer 6 small pyriform cell. The holding potential was −100 mV, and the cell was bathed in 0 Mg^{2+} buffer. *B,* A current–voltage plot for AMPA-evoked (*open circles*) and NMDA-evoked (*solid circles*) currents recorded in 3 mM Mg^{2+} bathing saline. Each point is the average of three agonist-evoked currents at the indicated holding potential from the same cell; the error bars represent the SEM. The *I–V* curve for the NMDA-evoked currents shows a pronounced inflection between −80 and −40 mV, while the *I–V* curve for the AMPA-evoked current can be fitted by a straight line.

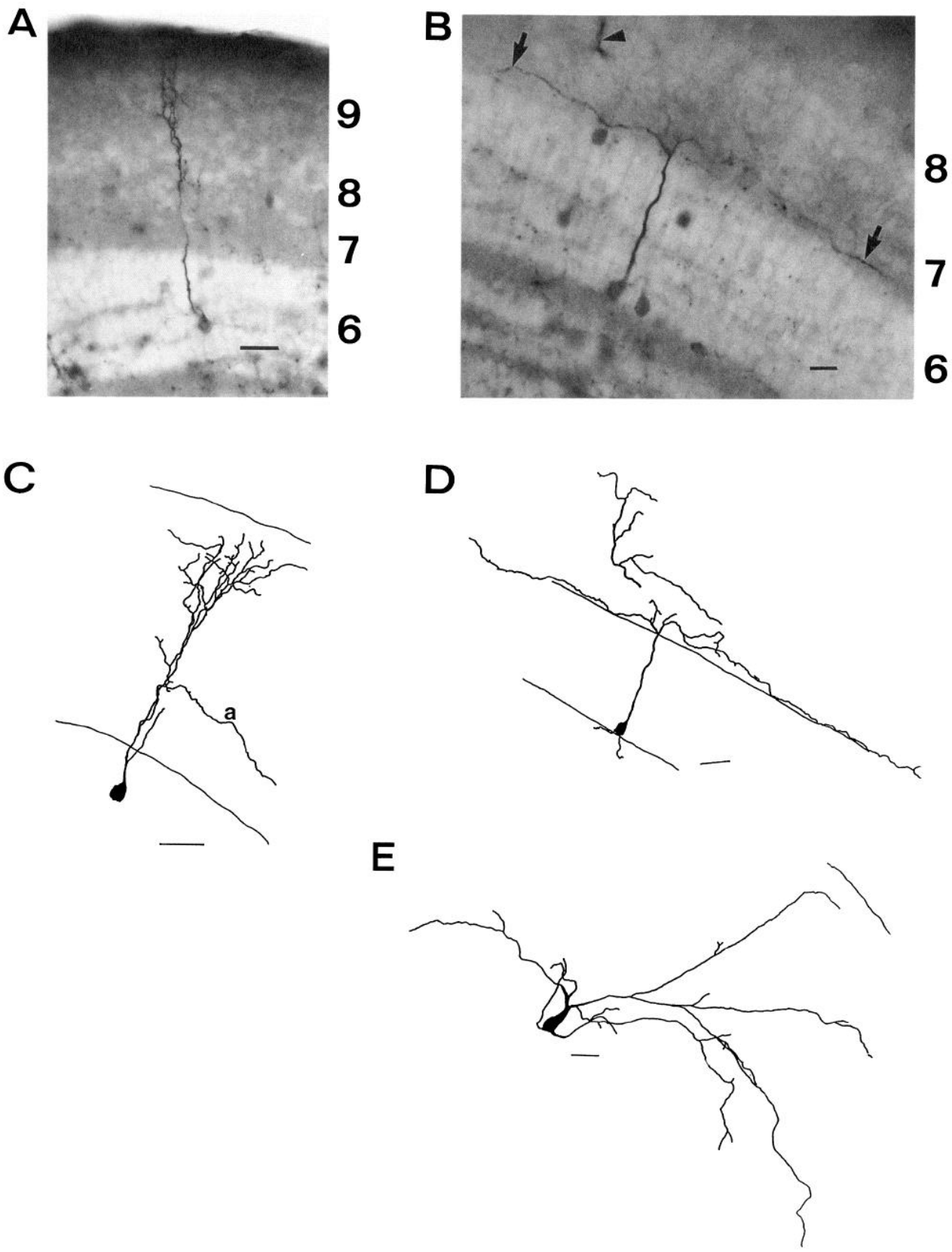

Figure 8. Examples of the morphology of voltage-clamped neurons in the tadpole optic tectum. *A,* Photomicrograph of a small pyriform neuron filled with biocytin and labeled with HRP-conjugated avidin. The soma was in layer 6, and there was one apical process extending toward the tectal surface, branching in layer 8–9 (much of the arbor lay outside the plane of focus). *B,* A photomicrograph of a pyramidal neuron filled and labeled as in *A*. The soma was in deep layer 6, and the cell extended a single process toward the surface. The process had two tangential branches,

layers 8 and 9. We observed two pyramidal cells (Fig. 8*B,D*), both of which had a medium-sized soma that extended radial processes that branched upon entering layer 8 of 9. Two tangentially oriented fine processes diverged from the apical dendrite of this cell and ran tangentially in layer 7. The fine caliber of these processes and their behavior in layer 7 suggest that they are axons. In general, we could not discriminate axons from dendrites. However, those axons that we could distinguish because of their small caliber and lack of branching appeared to extend off the proximal region of a primary dendritic process.

There were few obvious correlations of neuronal morphology with physiology: given the very small sample of nonpyriform cells (7 of 29), it would be difficult to detect any but very large differences. All cells appeared to have similar resting potentials, input resistances, and PSCs. However, one characteristic of ganglionic cells was that most (four of six) of them had very large (>500 pA at a holding potential of −60 mV) PSCs. Furthermore, within the pyriform cells there was a great deal of variability in the amplitude, duration, and overall shape of the PSC, which may reflect heterogeneity in this cell population. As for sensitivity of cell types to antagonists, at least one cell of each type responded to both DL-APV and CNQX. For both pyriform and ganglionic neurons, at least one cell responded to all three antagonists (two of two pyriform and one of one ganglionic). This indicates that at least two of three most common tectal neuron types can coexpress AMPA, NMDA, and $GABA_A$ receptors. Again, this apparent uniformity masks distinct quantitative differences in the effects of these drugs on the PSCs, particularly for the pyriform cell population.

Discussion

General. In previous studies, the response patterns of tectal neurons to visual or electrical stimulation have been examined in several lower vertebrates with conventional intracellular recording techniques (Matsumoto and Bando, 1980; Hardy et al., 1984, 1985; Antal et al., 1986; Leresche et al., 1986; Matsumoto et al., 1986). We chose to use patch-clamp techniques for voltage and current clamp, because most tectal neurons have small somata (6–10 μm diameter). Using conventional microelectrodes, such small neurons are difficult to penetrate without damage, and are thus difficult to maintain for enough time to examine drug effects on the PSP. Moreover, the problem of obtaining stable penetrations in these young animals is exacerbated by the fragility of the neurons. We used primarily voltage clamp, rather than current clamp, because the signal-to-noise ratio of whole-cell voltage clamp was considerably better than current clamp. We also wanted to gain information on the voltage-dependent properties of the PSCs in order to explore the contribution of NMDA receptor–mediated currents. We did not, however, expect to be able to perform rigorous quantitation of voltage-dependent properties of neuronal currents, because of inadequate space clamp of the elaborate and frequently very fine dendritic arbors of these neurons.

Nevertheless, using our approach, we were able to confirm our most important predictions about the tectal currents: that most tectal neurons are activated directly by retinotectal input, that these neurons have both non-NMDA and NMDA receptor–mediated currents contributing to their mono- and polysynaptic responses, that these NMDA receptor–mediated currents have a voltage dependency that is characteristic of such currents in other systems, and that GABAergic inhibitory currents are likely to modulate these excitatory currents.

Comparison with other studies. The resting potentials we measured were generally in the same range as those measured in the earlier intracellular studies of tectal neurons, although those from the earlier studies tended to be more depolarized, possibly due to damage to the neuronal membrane from the electrode penetration. Three types of responses of tectal neurons were typically observed in these earlier studies: (1) a single EPSP with one or two action potentials; (2) an EPSP, which sometimes resulted in an action potential, followed by an IPSP; or (3) an IPSP. Our studies using the high-Cl^- pipette solution to record PSCs appeared to be considerably different from these, as we saw only single long PSCs that reversed at about −5 mV. However, due to the high Cl^- concentration in the electrode, and thus in the cell, the reversal potential for Cl^- as well as for cations would be very close to this value. BMI application, and recordings using low-Cl^- solution in the electrode, proved that all neurons examined [nine of nine for BMI (see Fig. 6*D*) 10 of 10 for low-Cl^- solution] had a significant Cl^--based inhibitory component that was predominantly, but not exclusively, observed at longer latencies. These results, showing pronounced inhibition of postsynaptic responses in tectal neurons, are in essential agreement with those found in earlier studies.

Additionally, our results are consistent with and expand on the results obtained by Udin et al. (1992) on the effects of acute and chronic treatment with NMDA and DL-APV on adult *Rana pipiens* tectum. In that study, acute application of NMDA increased the spontaneous spike frequency in the tectum, but did not significantly affect the firing rate evoked via the isthmotectal projection; acute DL-APV decreased the spontaneous spike frequency and had a complex effect on the evoked spike firing rate: low concentrations of DL-APV (0.1 mM) decreased the evoked firing rate, but higher concentrations (0.5–1.0 mM) increased it. Implications of these complex effects on the evoked spikes are discussed below. Our data indicate that NMDA can directly depolarize tectal neurons, even near their resting potential (Fig. 7*A*; data from bath application of NMDA not shown). This direct depolarization could explain the increase in spontaneous firing, as neurons throughout the tectum would be depolarized and spike with NMDA application. Since DL-APV can reduce spontaneous activity, that implies that there is likely to be a significant amount of ongoing NMDA receptor activation even in the absence of visual stimuli, perhaps due to the firing of the "dimming detector" class of RGCs, as was suggested by Udin et al. (1992). Again, since we have shown that there is some

←

probably axons, in layer 7 (*arrows*), and also a radial branch (*arrowhead*). *C,* A camera lucida drawing of another small pyriform neuron that was filled and labeled as in *A*. As in *A,* the soma was in layer 6, and the single process extended to the tectal surface, branching in layer 8–9. Note that the fine process (*a*) was probably the neuron's axon. Note that this is not a complete reconstruction of the neuron's arbor; finer extensions of the processes probably continued somewhat farther. *D,* A camera lucida drawing of the same cell as in *B*. In addition to the processes indicated above, two short basal processes were evident, as was a fuller extent of the tangential and radial processes. Again, this is not a complete reconstruction of the cell: the tangential processes, in particular, probably extend considerably farther. *E,* A camera lucida drawing of a large ganglionic neuron that was filled with biocytin and labeled with FITC-conjugated avidin. In this cell the soma was in layer 7–8, and the cell extended very extensive processes tangentially and radially. As in *C,* this is not a complete reconstruction of the cell. Scale bars: *A* and *C–E,* 25 μm; *B,* 50 μm.

NMDA current even when tectal neurons are only slightly depolarized (Figs. 2*C*, 3*D*), this explanation is consistent with our data. In contrast to these changes detected by Udin et al. (1992) in response to acute DL-APV and NMDA treatment, chronic treatment with these drugs had little effect on spontaneous or evoked spikes, probably due to the very low concentrations of drug acting on tectal neurons ($\ll 1$ μM), or to some adjustment of neuronal responsiveness resulting from the continuous presence of the drug. Our data suggest that such low concentrations would be unlikely to affect the ability to activate retinotectal synapses, as there is initially very little NMDA receptor–mediated current associated with such activation. There is, however, a large contribution by non-NMDA current, which is unaffected by these drugs.

Studies of CNS neurons in mammals have suggested that in hippocampus, thalamus, and superior colliculus, monosynaptic EPSCs evoked by afferent stimulation are carried by both non-NMDA and NMDA receptors (Crunelli et al., 1987; Collingridge et al., 1988a,b; Kwon et al., 1991; Esguerra et al., 1992). However, in cortical neurons, it appears that NMDA receptors contribute primarily to polysynaptic PSCs while non-NMDA receptors contribute to both mono- and polysynaptic (Thompson, 1986; Sutor and Hablitz, 1989a,b; Hablitz and Sutor, 1990; but see also Fox et al., 1989, 1990). All these NMDA-mediated currents exhibit two distinguishing characteristics: (1) in the presence of external Mg^{2+}, their *I–V* curves show a region of negative slope conductance, reflecting the voltage-dependent block of the NMDA channel by Mg^{2+}; and (2) some component of the PSP/PSC is blocked by the NMDA antagonist DL-APV, at least at relatively depolarized potentials. Thus, at hyperpolarized holding potentials, nearly all of the PSC is carried by non-NMDA current, while at more depolarized potentials there is a significant NMDA current.

Excitation in retinotectal transmission. Our data indicate that there is a contribution by NMDA receptor currents to both mono- and polysynaptic PSCs. *I–V* curves from monosynaptic EPSCs show a region of voltage dependence in the *I–V* curve in most neurons in the presence of external Mg^{2+} (7 of 12 neurons; see Fig. 2*C*). This fact, coupled with the substantial reduction in the monosynaptic EPSC during DL-APV application (Fig. 2*B*), strongly indicates that NMDA current contributes significantly to the monosynaptic EPSC as soon as the tectal cell membrane is depolarized. That this is similar to data from mammalian superior colliculus (Hestrin, 1992) is not surprising, as the amphibian tectum is homologous to this structure. However, our data using maximal stimulation indicates that NMDA receptors are playing a significant role in polysynaptic and long-latency transmission as well. In these PSPs and PSCs, it is primarily the late component that exhibits a Mg^{2+}-dependent inflection in its *I–V* curve (Fig. 3*D*), and that is also reduced by DL-APV application (Figs. 4*B*, 6*C*). The relative contributions of polysynaptic and long-latency and slow monosynaptic currents to the late portion of the PSC recorded in tectal neurons are not known, and further experimentation would be necessary to dissect out and identify the various currents contributing to the long-latency component of the PSC. Nevertheless, at least some of the effects of DL-APV on the long-latency PSC are due to effects on polysynaptic current.

Another interesting observation is that not all tectal neurons seem to express both non-NMDA and NMDA receptors; a small fraction either did not respond to DL-APV application (Fig. 5) or to iontophoretically applied NMDA, or had no voltage dependence in the presence of Mg^{2+}. This implies that the subtypes of glutamate receptors may not be coexpressed in all cases, or that there may be differential regulation of the effectiveness of non-NMDA and NMDA receptor subtypes as has been suggested in other systems (Bekkers and Stevens, 1989; Jones and Baughman, 1991).

Inhibition. In addition to excitatory receptor systems, our data suggest that all tectal neurons also express strong, chloride-dependent inhibitory currents when activated by greater than minimal stimulation (compare Fig. 3*A,B*; see Fig. 6). Both kinetic data from experiments using low-Cl^- solution (Fig. 3*B*), where IPSCs can be differentiated from EPSCs, and pharmacological data from BMI application (Figs. 4*C*, 6*D*) support this idea. The bulk of this inhibition thus appears to be based on $GABA_A$-type Cl^- currents. Since the approximate reversal potential of the late IPSC (−41 mV) is relatively near the average resting potential of tectal neurons (−50 mV), it appears that the bulk of this inhibition occurs by shunting of the excitatory currents (Eccles, 1964). This hypothesis is further supported by the observations that BMI application frequently causes a significant increase in the PSC (Figs. 4*C*, 6*D*), and that iontophoretic application of GABA along with AMPA or NMDA completely blocked the excitatory current produced by either of those agonists. Possible contributions of a late $GABA_B$ receptor–mediated current (Connors et al., 1988; Dutar and Nicoll, 1988) would not have been seen in our experiments, because the $GABA_B$ current is a K^+ current (Inoue et al., 1985; Newberry and Nicoll, 1985), and is thus blocked by the Cs^+ in our recording electrodes.

In 3 of 15 cases, DL-APV application actually increased the early component of the PSC by up to 2.5 times. This observation suggested that DL-APV application was actually disinhibiting the neuron from which we were recording. This would imply that NMDA receptors were relatively highly concentrated on inhibitory interneurons, as has been observed in cerebellar slices (Llano et al., 1991). Previous studies in the optic tectum have also suggested that NMDA receptors might indeed be concentrated on inhibitory neurons. Electrically evoked field potentials recorded extracellularly both in intact tecta (Debski and Constantine-Paton, 1988) and in slices from tecta (Hickmott and Constantine-Paton, 1989) exhibit an increase in some postsynaptic components of the field potential, rather than the expected decrease in response to DL-APV. Additionally, Udin et al. (1992) found that acute application of high concentrations (0.5–1.0 mM) of DL-APV to the tectum also caused a significant increase in the spike firing rate evoked by light flashes in the tecta of adult *Rana pipiens*, while lower concentrations (0.1 mM) caused a decrease. Thus, these experiments blocking a presumably excitatory receptor led to an increase in the response, implying that some concentration of DL-APV was blocking inhibition more effectively than excitation. However, we have obtained no direct evidence on the relative contributions of non-NMDA and NMDA receptors on inhibitory versus excitatory neurons due to the difficulty in differentiating these types of neurons from each other in physiological experiments.

Implications for tectal activation and processing. These data have implications for transmission and processing in the tectum, as well as development of the retinotectal pathway. The onset of retinotectal transmission appears to be mediated primarily by non-NMDA glutamate receptors. When tectal neurons were held near the resting potential (−60 mV), only a few monosynaptic EPSCs were sensitive to DL-APV. However, CNQX com-

pletely blocked the monosynaptic EPSC in all such neurons tested. Additionally, when activated maximally, DL-APV had a much smaller effect on the early portion of the PSC, which consists primarily of a summation of monosynaptic currents, than on the late portion, which contains polysynaptic as well as long-latency currents (Figs. 4*B*, 6*C*; Table 1). Thus, we believe that for most tectal neurons the initial stages of retinotectal transmission are mediated by non-NMDA glutamate receptors. The situation for retinal synapses activated during depolarization and for polysynaptic transmission within the tectum is quite different: both are significantly antagonized by DL-APV, and exhibit a region of voltage dependence in their *I–V* curves that is evident only in the presence of external Mg^{2+}. For the polysynaptic currents this reduction occurs even when the patched cell is held at hyperpolarized holding potentials, indicating that the reduction reflects block of NMDA receptors on neurons that are in the circuit between the optic tract afferents and the patched cell. Considering that a great deal of this polysynaptic input to the neuron seems to be inhibitory, or at least under inhibitory control, it appears that inhibitory interneurons may express a relatively high concentration of NMDA receptors. The marked difference in the degree of NMDA receptor activation between mono- and polysynaptic responses of tectal neurons could also reflect polysynaptic feedback collateral excitation, which is expected in many tectal neurons (Székely et al., 1973). Such collateral excitation would tend to depolarize neurons during the longer-latency parts of the PSC, thus relieving the Mg^{2+} block on the NMDA channels. It could also depolarize neurons during sustained activation by RGC synapses, leading to an increase in the NMDA receptor–mediated current in these monosynaptic responses as well.

Developmental implications. There is a growing body of evidence that implicates the NMDA receptor in the activity-dependent development of maps in a number of regions in the brain, including the retinotectal (Cline et al., 1987; Cline and Constantine-Paton, 1989, 1990; Schmidt, 1990) and isthmotectal (Scherer and Udin, 1989) projection in lower vertebrates, and also in the retinocollicular (Simon et al., 1992) and thalamocortical projection of mammals (Kleinschmidt et al., 1987; Bear et al., 1990). To play such a critical role in the refinement of the retinotectal map, we hypothesized that there should be functional NMDA receptors at retinotectal synapses. If, however, these receptors were responsible for a significant fraction of normal transmission, it would be difficult to attribute to them a role as specific detectors of correlated activity, rather than a more general role in synaptic activation.

Our data provide support for the idea that NMDA receptors are present at retinotectal synapses (see Fig. 2*B*), but are mostly blocked by Mg^{2+} when neurons are near resting potential (Fig. 2*C*). Thus, our data are consistent with the possibility that NMDA receptors play little role in the initial phases of retinotectal transmission, but are activated only during temporal or spatial summation of excitatory responses, which leads to increased depolarization of tectal neurons. Furthermore, correlated activity among RGCs synapsing on any given tectal neuron would greatly increase the amount of depolarization in that neuron, and would thus result in increased NMDA receptor activation in that neuron. Thus, chronic treatment with DL-APV would have a smaller effect on the initial phases of retinotectal transmission than on those components of transmission caused by highly correlated (i.e., neighboring) RGCs. The effects of chronic DL-APV application on the tectum seen at the anatomical level (Cline et al., 1987; Cline and Constantine-Paton, 1989, 1990) would thus primarily reflect effects on these highly correlated RGCs. Note that our data do not rule out the possibility that the reduction in overall depolarization reduces activity-dependent plasticity by decreasing the amount of Ca^{2+} entry through voltage-gated Ca^{2+} channels or other sources, rather than specifically through the NMDA channel (cf. Fields et al., 1991; for review, see Fields and Nelson, 1992). However, the observation that specific block of the NMDA channel blocks activity-dependent plasticity (Cline et al., 1987) implies that Ca^{2+} entry through the NMDA channel is indeed important. An interesting possibility that results from our finding a large amount of NMDA receptor activity in normal polysynaptic transmission is that NMDA receptor activation may also be important for the proper development of specific connections within the tectum, rather than just being important for afferent segregation.

From these studies, it is also apparent that inhibition is likely to be important in modulating developmental events in the tectum that are dependent on NMDA receptor activation. GABA-mediated inhibition of the PSC is rapid and powerful, and can apparently affect even early portions of the PSP/PSC (see Figs. 3*B*, 4*C*, 6*D*). For example, inhibition will control the effective duration of depolarization in the neuron, and thus will determine the time window where the NMDA conductances can be activated by subsequent stimuli. Decreases in inhibition would be expected to produce longer-lasting depolarizations for a given amount of RGC activation, and could therefore increase the amount of excitatory temporal summation produced by afferent stimulation. This would then decrease the degree of correlation between inputs necessary to activate NMDA conductances to a level required to stabilize the active inputs.

Relating morphology to physiology. It was difficult to relate cell morphology to physiology in this system, primarily due to the small sample size ($n = 7$) of nonpyriform cells obtained. Also, electrical stimulation masks differences in tectal responses that would be apparent in responses driven by visual stimulation. However, it does appear that pyriform cells have very heterogeneous response properties, without a great difference in morphology. There are two main reasons for this. (1) Pyriform cells can be classified into subgroups by soma size (Székely and Lázár, 1976), arbor morphology (Antal et al., 1986), or presence or absence of dendritic spines (Antal et al., 1986). No attempt was made to differentiate possible subtypes of pyriform cells in this study. In fact, very few tectal neurons have spine-like appendages in these young animals. (2) Pyriform cells are thought to play a number of roles in the tectal circuitry. They are thought to be both local and longer-range interneurons, and projection neurons (Lázár, 1984). For example, nonspiking pyriform cells have been postulated to act as very local interneurons, probably within a "tectal column" (a hypothetical tectal functional unit; see Székely and Lázár, 1976; Arbib and Lara, 1982; Lara et al., 1982; Lázár, 1984), while spiking neurons could project within columns, to other tectal columns, or outside the tectal lobe. Ganglionic and pyramidal cells are thought to be the main output elements of the tectum, sending efferents primarily through layer 7 (Székely and Lázár, 1976; Lázár, 1984). It is difficult to determine possible output characteristics of these neurons without examining spiking patterns in detail, and without data on the same cells' responses to visual stimulation. However, the fact that four of six ganglionic neurons had very large PSCs could indicate that these cells have relatively robust output.

Alternatively, the size of these PSCs could merely reflect the larger size of these cells, which might allow them to receive more inputs, resulting in a larger PSC.

Conclusions. In summary, our results show that tectal neurons immediately postsynaptic to the optic nerve input in the tecta of developing tadpoles and young postmetamorphic frogs have both excitatory and inhibitory amino acid–mediated components of their response to optic tract stimulation. In addition, in the majority of cells, both NMDA and non-NMDA ionotropic receptors contribute to the excitatory component of their response. These NMDA channels also express the characteristic voltage dependence that would make them uniquely suitable for detecting patterns of correlated afferent activity. Moreover, bath application of DL-APV, the specific blocker of the NMDA channel, though clearly functioning to decrease an excitatory component of the response, fails to inhibit retinotectal synaptic transmission completely, and in a few cells appears to facilitate excitation, possibly by blocking a polysynaptic inhibitory pathway. Taken together, these results indicate that previous studies using chronic tectal application of DL-APV or NMDA in nanomolar ranges (Cline and Constantine-Paton, 1987, 1989; Debski et al., 1991) at the same ages probably did not produce the observed structural effects by simply blocking ongoing retinotectal synaptic transmission. Rather, highly correlated inputs, which would produce the largest depolarizations of tectal neurons, were likely to be most affected by these treatments. Thus, these physiological data are consistent with the hypothesis that an NMDA receptor–driven mechanism serves to stabilize these correlated inputs selectively, thereby producing the point-to-point order in the retinotectal map.

References

Antal M, Matsumoto N, Székely G (1986) Tectal neurons of the frog: intracellular recording and labelling with cobalt electrodes. J Comp Neurol 246:238–253.

Arbib MA, Lara R (1982) A neural model of the interaction of tectal columns in prey-catching behavior. Biol Cybern 44:185–196.

Arnett DW (1978) Statistical dependence between neighboring retinal ganglion cells in goldfish. Exp Brain Res 32:49–53.

Artola A, Singer W (1987) Long-term potentiation and NMDA receptors in rat visual cortex. Nature 330:649–652.

Bear M, Kleinschmidt A, Gu Q, Singer W (1990) Disruption of experience-dependent modifications in striate cortex by infusion of an NMDA receptor antagonist. J Neurosci 10:909–924.

Bekkers JM, Stevens CF (1989) NMDA and non-NMDA receptors are co-localized at individual excitatory synapses in cultured rat hippocampus. Nature 341:230–233.

Blanton MG, LoTurco JJ, Kriegstein AR (1989) Whole cell recordings from neurons in slices of reptilian and mammalian cortex. J Neurosci Methods 30:203–210.

Bliss TVP, Lomo T (1973) Long-lasting potentiation of synaptic transmission in the dentate area of the anaesthetized rabbit following stimulation of the perforant path. J Physiol (Lond) 232:331–356.

Bonhoeffer F, Huf J (1982) *In vitro* experiments on axon guidance demonstrating an anterior–posterior gradient on the tectum. EMBO J 1:427–431.

Brown TH, Chapman PFE, Kairiss W, Keenan CL (1988) Long-term synaptic potentiation. Science 242:724–728.

Cline HT, Constantine-Paton M (1987) The role of the NMDA receptor in eye-specific segregation in three eyed tadpoles. Soc Neurosci Abstr 13:1691.

Cline HT, Constantine-Paton M (1989) NMDA receptor antagonists disrupt the retinotectal topographic map. Neuron 3:413–426.

Cline HT, Constantine-Paton M (1990) NMDA receptor drug treatment alters RGC terminal morphology *in vivo*. J Neurosci 10:1197–1216.

Cline HT, Debski E, Constantine-Paton M (1987) NMDA receptor antagonist desegregates eye specific stripes. Proc Natl Acad Sci USA 84:4342–4345.

Collingridge GL, Herron CE, Lester RAJ (1988a) Synaptic activation of *N*-methyl-D-aspartate receptors in the Schaffer collateral–commissural pathway of rat hippocampus. J Physiol (Lond) 399:283–300.

Collingridge GL, Herron CE, Lester RAJ (1988b) Frequency-dependent *N*-methyl-D-aspartate receptor–mediated synaptic transmission. J Physiol (Lond) 399:301–312.

Connors BW, Malenka RC, Silva LR (1988) Two inhibitory postsynaptic potentials, and $GABA_A$ and $GABA_B$ receptor–mediated responses in neocortex of rat and cat. J Physiol (Lond) 406:443–468.

Constantine-Paton M (1990) The NMDA receptor as a mediator of activity-dependent synaptogenesis in the developing brain. Cold Spring Harbor Symp Quant Biol 55:431–443.

Crunelli V, Forda S, Kelly JS (1984) The reversal potential of excitatory amino acid action on granule cells of the rat dentate gyrus. J Physiol (Lond) 351:327–342.

Crunelli V, Kelly JS, Leresche N, Pirchio M (1987) On the excitatory postsynaptic potential evoked by stimulation of the optic tract in the rat lateral geniculate nucleus. J Physiol (Lond) 384:603–618.

Debski EA, Constantine-Paton M (1988) The effects of glutamate receptor agonists and antagonists on the evoked tectal potential in *Rana pipiens*. Soc Neurosci Abstr 14:674.

Debski EA, Cline HT, Constantine-Paton M (1987) Kynurenic acid blocks retinal-tectal transmission in *Rana pipiens*. Soc Neurosci Abstr 13:1691.

Debski EA, Cline HT, McDonald JW, Constantine-Paton M (1991) Chronic application of NMDA decreases the NMDA sensitivity of the evoked potential in the frog. J Neurosci 11:2947–2957.

Dutar P, Nicoll RA (1988) A physiological role for $GABA_B$ receptors in the central nervous system. Nature 332:156–158.

Eccles JC (1964) The physiology of synapses. Berlin: Springer.

Esguerra M, Kwon YH, Sur M (1992) Retinogeniculate EPSPs recorded intracellularly in the ferret lateral geniculate nucleus *in vitro*: role of NMDA receptors. Vis Neurosci 8:545–555.

Ewert JP (1984) Tectal mechanisms that underlie prey-catching and avoidance behaviors in toads. In: Comparative neurology of the optic tectum (Vanegas H, ed), pp 247–416. New York: Plenum.

Fields RD, Nelson PG (1992) Activity-dependent development of the vertebrate nervous system. Int Rev Neurobiol 34:133–214.

Fields RD, Chang Y, Nelson PG (1991) Calcium, network activity, and the role of NMDA channels in synaptic plasticity *in vitro*. J Neurosci 11:134–146.

Fox K, Sato H, Daw N (1989) The location and function of NMDA receptors in cat and kitten visual cortex. J Neurosci 9:2443–2454.

Fox K, Sato H, Daw N (1990) The effect of varying stimulus intensity on NMDA-receptor activity in cat visual cortex. J Neurophysiol 64: 1413–1428.

Fox K, Daw N, Sato H, Czepita D (1991) Dark-rearing delays the loss of NMDA-receptor function in kitten visual cortex. Nature 350:342–344.

Fraser SE (1985) Cell interactions involved in neuronal patterning: an experimental and theoretical approach. In: Molecular bases on neural development (Edelman GM, Gall WE, Cowan WM, eds), pp 481–507. New York: Wiley.

Freeman JA, Norden JJ (1984) Neurotransmitters in the optic tectum of nonmammalians. In: Comparative neurology of the optic tectum (Vanegas H, ed), pp 469–546. New York: Plenum.

Grusser O-J, Grüsser-Cornehls U (1976) Neurophysiology of the anuran visual system. In: Frog neurobiology (Llinas R, Precht W, eds), pp 297–385. New York: Springer.

Hablitz JJ, Sutor B (1990) EPSPs in rat neocortical neurons *in vitro*. III. Effects of a quinoxalinedione non-NMDA receptor antagonist. J Neurophysiol 64:1282–1290.

Hardy O, Leresche N, Jassik-Gerschenfeld D (1984) Postsynaptic potentials in neurons of the pigeon's optic tectum in response to afferent stimulation from the retina and other visual structures: an intracellular study. Brain Res 311:65–74.

Hardy O, Leresche N, Jassik-Gerschenfeld D (1985) Morphology and laminar distribution of electrophysiologically identified cells in the pigeon's optic tectum: an intracellular study. J Comp Neurol 233: 390–404.

Hebb DO (1949) Organization of behavior. New York: Wiley.

Hestrin S (1992) Developmental regulation of NMDA receptor–mediated synaptic currents at a central synapse. Nature 357:686–689.

Hestrin S, Nicoll RA, Perkel DJ, Sah P (1990a) Analysis of excitatory synaptic action in pyramidal cells using whole-cell recording from rat hippocampal slices. J Physiol (Lond) 422:203–225.

Hestrin S, Sah P, Nicoll RA (1990b) Mechanisms generating the time course of dual component excitatory synaptic currents recorded in hippocampal slices. Neuron 5:246–253.

Hickmott PW, Constantine-Paton M (1989) Pharmacology of retinotectal transmission in *Rana pipiens* tectal slices. Soc Neurosci Abstr 15:979.

Hickmott PW, Constantine-Paton M (1990) Physiology and morphology of neurons in *Rana pipiens* tectal slices. Soc Neurosci Abstr 16:985.

Hickmott PW, Constantine-Paton M (1991) Quantitative analysis of agonist-evoked currents in identified tectal neurons of *Rana pipiens*. Soc Neurosci Abstr 17:1134.

Horikama K, Armstrong WE (1988) A versatile means of intracellular labelling: injection of biocytin and its detection with avidin conjugates. J Neurosci Methods 25:1–11.

Inoue M, Matsuo T, Ogata N (1985) Possible involvement of K^+-conductance in the action of gamma-aminobutyric acid in the guinea pig hippocampus. Br J Pharmacol 86:515–524.

Jones KA, Baughman RW (1991) Both NMDA and non-NMDA subtypes of glutamate receptors are concentrated at synapses on cerebral cortical neurons in culture. Neuron 7:593–603.

Katz B, Miledi R (1965) The effect of temperature on the synaptic delay at the neuromuscular junction. J Physiol (Lond) 181:656–670.

Kleinschmidt A, Bear MF, Singer W (1987) Blockade of NMDA receptors disrupts experience-dependent plasticity of kitten striate cortex. Science 238:355–358.

Kuljis RO, Krause JE, Karten HJ (1984) Peptide-like immunoreactivity in anuran optic nerve fibers. J Comp Neurol 226:222–237.

Kwon YH, Esguerra M, Sur M (1991) NMDA and non-NMDA receptors mediate visual responses of neurons in the cat's lateral geniculate nucleus. J Neurophysiol 66:414–428.

Langdon RB, Freeman JA (1986) Antagonists of glutaminergic neurotransmission block retinotectal transmission in goldfish. Brain Res 398:169–174.

Langdon RB, Freeman JA (1987) Pharmacology of retinotectal transmission in the goldfish: effects of nicotinic ligands, strychnine, and kynurenic acid. J Neurosci 7:760–773.

Lara R, Arbib MA, Cromarty AS (1982) The role of the tectal column in facilitation of amphibian prey-catching behavior: a neural model. J Neurosci 2:521–530.

Law MI, Constantine-Paton M (1982) A banded distribution of retinal afferents within layer 9A of the normal frog optic tectum. Brain Res 247:201–208.

Lázár G (1984) Structure and connections of the frog optic tectum. In: Comparative neurology of the optic tectum (Vanegas H, ed), pp 185–210. New York: Plenum.

Leresche N, Hardy O, Audinat E, Jassik-Gerschenfeld D (1986) Synaptic transmission of excitation from the retina to cells in the pigeon's optic tectum. Brain Res 365:138–144.

Levine R (1984) Neuronal plasticity in the optic tectum of amphibians. In: Comparative neurology of the optic tectum (Vanegas H, ed), pp 469–546. New York: Plenum.

Llano I, Marty A, Armstrong CM, Konnerth A (1991) Synaptic- and agonist-induced excitatory currents of Purkinje cells in rat cerebellar slices. J Physiol (Lond) 434:183–213.

Maffei L, Galli-Resta L (1990) Correlation in the discharges of neighboring retinal ganglion cells during prenatal life. Proc Natl Acad Sci USA 87:2861–2864.

Mastronarde DN (1983a) Correlated firing of cat retinal ganglion cells. I. Spontaneously active inputs to X- and Y-cells. J Neurophysiol 49: 303–324.

Mastronarde DN (1983b) Correlated firing of cat retinal ganglion cells. II. Responses of X- and Y-cells to single quantal events. J Neurophysiol 49:325–349.

Matsumoto N, Bando T (1980) Excitatory synaptic potentials and morphological classification of tectal neurons of the frog. Brain Res 192:39–48.

Matsumoto N, Schwippert WW, Ewert J-P (1986) Intracellular activity of morphologically identified neurons of the grass frog's optic tectum in response to moving configurational visual stimuli. J Comp Physiol 159:721–739.

Mayer ML, Westbrook GL (1987) The physiology of excitatory amino acids in the vertebrate central nervous system. Prog Neurobiol 28: 197–276.

Mayer ML, Westbrook GL, Guthrie PB (1984) Voltage-dependent block by Mg^{++} of NMDA responses in spinal cord neurons. Nature 309:261–263.

Meister M, Wong ROL, Baylor DA, Shatz CJ (1991) Synchronous bursts of action potentials in ganglion cells of the developing mammalian retina. Science 252:939–943.

Meyer RL (1982) Tetrodotoxin blocks the formation of ocular dominance columns in goldfish. Science 218:589–591.

Miller KD, Chapman B, Stryker MP (1989) Visual responses in adult cat visual cortex depend on *N*-methyl-D-aspartate receptors. Proc Natl Acad Sci USA 86:5183–5187.

Newberry NR, Nicoll RA (1985) Comparison of the action of baclofen with gamma-aminobutyric acid on rat hippocampal pyramidal cells *in vitro*. J Physiol (Lond) 360:161–185.

Reh TA, Constantine-Paton M (1985) Eye-specific segregation requires neural activity in three-eyed *Rana pipiens*. J Neurosci 5:1132–1143.

Reiter HO, Stryker MP (1988) Neural plasticity without postsynaptic action potentials: less-active inputs become dominant when kitten visual cortical cells are pharmacologically inhibited. Proc Natl Acad Sci USA 85:3623–3627.

Scherer WJ, Udin SB (1989) *N*-methyl-D-aspartate antagonists prevent interaction of binocular maps in *Xenopus* tectum. J Neurosci 9:3837–3843.

Schmidt JT (1990) Long-term potentiation and activity dependent retinotopic sharpening in the regenerating retinotectal projection of goldfish: common sensitive periods and sensitivity to NMDA blockers. J Neurosci 10:233–246.

Schmidt JT, Eisele LE (1985) Stroboscopic illumination and dark rearing block the sharpening of the regenerated retinotectal map in goldfish. Neuroscience 14:535–546.

Sharma SC, Romeskie M (1984) Plasticity of retino-tectal connections in teleosts. In: Comparative neurology of the optic tectum (Vanegas H, ed), pp 163–184. New York: Plenum.

Shaw C, Cynader M (1984) Disruption of cortical activity prevents ocular dominance changes in monocularly deprived kittens. Nature 308:731–734.

Simon DK, Prusky GT, O'Leary DDM, Constantine-Paton M (1992) *N*-methyl-D-aspartate receptor antagonists disrupt the formation of a mammalian neural map. Proc Natl Acad Sci USA 89:10593–10597.

Stahl B, von Boxverg Y, Muller B, Walter J, Schwarz U, Bonhoeffer F (1990) Directional cues for retinal axons. Cold Spring Harbor Symp Quant Biol 55:351–357.

Stryker MP, Harris WA (1986) Binocular impulse blockade prevents the formation of ocular dominance columns in cat visual cortex. J Neurosci 6:2117–2133.

Sutor B, Hablitz JJ (1989a) EPSPs in rat neocortical neurons *in vitro*. I. Electrophysiological evidence for two distinct EPSPs. J Neurophysiol 61:607–620.

Sutor B, Hablitz JJ (1989b) EPSPs in rat neocortical neurons *in vitro*. II. Involvement of *N*-methyl-D-aspartate receptors in the generation of EPSPs. J Neurophysiol 61:621–634.

Székely G, Lázár G (1976) Cellular and synaptic architecture of the optic tectum. In: Frog neurobiology (Llinas R, Precht W, eds), pp 407–434. New York: Springer.

Székely G, Setalo G, Lázár G (1973) Fine structure of the frog's optic tectum: optic fibre termination layers. J Hirnforsch 14:189–225.

Taylor AC, Kollros JJ (1946) Stages in the normal development of *Rana pipiens* larvae. Anat Rec 94:7–23.

Thompson AM (1986) A magnesium-sensitive postsynaptic potential in rat cerebral cortex resembles neural responses to *N*-methylaspartate. J Physiol (Lond) 370:531–550.

Udin SB, Fawcett JW (1988) Formation of topographic maps. Annu Rev Neurosci 11:289–327.

Udin SB, Scherer WJ, Constantine-Paton M (1992) Physiological effects of chronic and acute application of *N*-methyl-D-aspartate and 5-amino-phosphonovaleric acid to the optic tectum of *Rana pipiens* frogs. Neuroscience 49:739–747.